Cation occupancies in Mg, Co, Ni, Zn, Al ferrite spinels: a multi-element EXAFS study

2007 J. Phys.: Condens. Matter 19 076214

(http://iopscience.iop.org/0953-8984/19/7/076214)

IOP PUBLISHING JOURNAL OF PHYSICS: CONDENSED MATTER

J. Phys.: Condens. Matter **19** (2007) 076214 (25pp) doi:10.1088/0953-8984/19/7/076214

Cation occupancies in Mg, Co, Ni, Zn, Al ferrite spinels: a multi-element EXAFS study

C M B Henderson[1,2], J M Charnock[1,2] and D A Plant[2]

[1] Synchrotron Radiation Department, Daresbury Laboratory, CCLRC, Warrington WA4 4AD, UK
[2] Williamson Research Centre, School of Earth, Atmospheric and Environmental Sciences (SEAES), University of Manchester, Manchester M13 9PL, UK

Received 18 December 2006, in final form 8 January 2007
Published 2 February 2007
Online at stacks.iop.org/JPhysCM/19/076214

Abstract

The distribution of cations between tetrahedral (A) sites and octahedral (B) sites in ferrite spinels has been studied using K-edge x-ray absorption spectroscopy. The samples include natural and synthetic end-member magnetites (Fe_3O_4), a natural Mn- and Zn-rich magnetite (franklinite) and synthetic binary, ternary and quaternary ferrites of stoichiometry $M^{2+}M^{3+}_2O_4$, where M^{2+} = Mg, Co, Ni, Zn and M^{3+} = Fe, Al. XAS data were obtained for all metals. Complete, unfiltered, EXAFS spectra were refined to determine the percentage distribution of each element over the A and B sites and these data were combined with microprobe analyses to quantify the tetrahedral occupancy for each element in each sample. Measured site occupancies and an internally consistent set of $(M–O)^A$ and $(M–O)^B$ bond lengths were used to calculate unit-cell parameters, which show excellent agreement with measured values, pointing to the reliability of the measured occupancy factors. The average occupancies determined for the tetrahedral sites in ferrites are (atoms per formula unit) Mg 0.44, Co 0.24, Ni 0.11, Zn 0.76, Al 0.11 and Fe^{3+} 0.92–0.19. The wide range found for Fe^{3+} is consistent with it playing a relatively passive role by making good any A-site deficit left by the other competing cations.

1. Introduction

The material science (*sensu lato*) literature is rich in papers dealing with the structural, physical and chemical properties of phases belonging to the spinel structure type, with general chemical formulae $M^{2+}O{\cdot}M^{3+}_2O_3$ (where M^{2+} = Mg, Mn, Fe, Co, Ni, Cu, Zn and M^{3+} = Al, V, Cr, Mn, Fe, Co). The striking feature of the iron-rich analogues (ferrite spinels) is their ferrimagnetism. End members and solid solutions within these chemical systems are easily synthesized, and because of their physical and electronic properties are very widely used as technological materials (e.g. in magnetic recording media, batteries, catalysts and pigments). Spinels occur as natural minerals (e.g. end-members spinel $MgAl_2O_4$, hercynite $FeAl_2O_4$, gahnite $ZnAl_2O_4$, magnetite Fe_3O_4, trevorite $NiFe_2O_4$ and coulsonite FeV_2O_4), many of

which are complex solid solutions (e.g. chromite $(Fe, Mg)^{2+}(Cr, Al, Fe)^{3+}O_4$ and jacobsite $(Mn, Fe, Mg)^{2+}(Fe, Mn)^{3+}O_4$). Ti-bearing spinels (titanomagnetite) occur naturally as solid solutions between magnetite and ulvöspinel ($Fe_2^{2+}TiO_4$). Oxidized analogues of Fe^{2+}-bearing spinels are also known (e.g. maghemite $Fe_{2.66}^{3+}O_4$ (γ-Fe_2O_3) and titanomaghemite). Spinel-group minerals in metamorphic and igneous rocks are useful indicators of the redox conditions of rock formation (see, e.g., Frost 1991, Frost and Lindsley 1991) and the occurrence of magnetite is particularly important for palaeomagnetic reconstructions of the drifting continents over geological time (O'Reilly 1994). In addition, the importance of the presence of spinel-type phases in the Earth's mantle has recently led to high-pressure experimental studies of phase transformations in magnesioferrite ($MgFe_2O_4$) (Winell *et al* 2006) and measurements of sound velocities and elastic constants in gahnite ($ZnAl_2O_4$) (Reichmann and Jacobsen 2006).

The crystal chemistry and structure of spinels were reviewed comprehensively by Lindsley (1976) and Waychunas (1991). The oxygens form a face-centred, cubic close-packed array in which cations occupy one-quarter of the tetrahedral sites (A sub-lattice) and one-half of the octahedral sites (B sub-lattice). *Normal* spinels are characterized by the cation distribution $(M^{2+})^A(M^{3+}M^{3+})^BO_4$ while *inverse* spinels have the general formula $(M^{3+})^A(M^{2+}M^{3+})^BO_4$. Most spinels show non-convergent disorder of cations over the tetrahedral and octahedral sites and can be described using an inversion parameter (i) and the formula $(M_{1-i}^{2+}M_i^{3+})^A(M_i^{2+}M_{2-i}^{3+})^BO_4$, where $i = 0$ for an end-member normal spinel and $i = 1$ for a completely inverse spinel. A fully disordered spinel would have $i = 0.666$. The degree of order may also be defined as an order parameter (Q) which varies from $Q = 1$ for completely ordered normal spinel to $Q = 0$ for a fully disordered arrangement, and to $Q = -0.5$ for an inverse spinel. The relationship between Q and i can be denoted $Q = 1 - 3/2i$ (Redfern *et al* 1999). The degree of disorder depends on the temperature (and pressure) of equilibration and it has been shown for synthetic samples that the equilibrium order is only easily quenchable from annealing temperatures below ~900–1000 °C (Millard *et al* 1992), thus the highest temperature equilibrium disorder properties can only be determined using *in situ* methods (see, e.g., Harrison *et al* 1998, Redfern *et al* 1999, Martignano *et al* 2006). Although some information is available regarding the dependence of the degree of disorder on pressure at room temperature (e.g. Pavese *et al* 1999), very few determinations have been made at elevated T and P. However, Méducin *et al* (2004) studied MgA_2O_4 with *in situ* neutron diffraction methods to show that high pressure 'favours disordering towards the inverse structure'. In addition, Turkin and Drebushchak (2005) used XRD on magnesioferrite ($MgFe_2O_4$) samples rapidly quenched from high-P/T conditions, to deduce that the inverse spinel structure is favoured at higher pressure.

The physical properties of spinels are crucially dependent on the ordering of cations and much attention has been paid to determining this aspect of the structures of synthetic and natural samples. X-ray and neutron diffraction methods have been used to determine ordering over the tetrahedral and octahedral sites (see representative data summarized in table 1), but the data are only unambiguous for binary metal compounds and where the scattering properties of the two metals are sufficiently different. Natural spinels are often chemically complex, making it impossible to determine site occupancies directly, although modelling approaches combining refined *mean* cation–oxygen distances, cell parameters, oxygen coordinates and cation sizes have provided useful data for samples of known chemical composition (see, e.g., Carbonin *et al* 1996, Lucchesi *et al* 1999, Uchida *et al* 2005). Reliable determination of metal oxidation states is even more difficult, although iron (^{57}Fe) Mössbauer spectroscopy provides important information on valency, coordination and magnetic ordering (see, e.g., O'Neill 1992, Carbonin *et al* 1996), but this technique cannot be used to distinguish iron atoms in octahedral sites where Fe^{3+} and Fe^{2+} are hybridized. In addition, ^{27}Al NMR has been used to provide

Table 1. Representative published cation site ordering data measured at room temperature on natural samples or on synthetic samples quenched from different temperatures.

Sample name	$M^{2+}M_2^{3+}O_4$	Synthesis or annealing temp	i (M^{3+} in [A]); [x^{Me}; % total element in A]	M^{2+} in [B]	Cell edge (Å)	Method	Source
MgFe	$MgFe_2O_4$	400	0.90; [Mg 10]	0.9	8.3805	Powder XRD and	O'Neill *et al* (1992)
		1200	0.71; [Mg 29]	0.71	8.3998	^{57}Fe Mössbauer	
	$Mg_{1.02}Fe_{1.988}O_4$	1200 then 700 then 300	0.85; [Mg 15]	0.43	8.3600	Single crystal XRD and NMR	Nakatsuka *et al* (2004)
	$MgFe_2O_4$	900	0.75; [Mg 25]	0.75	8.399	Curie temperature measurements	Harrison and Putnis (1999)
		500	0.89; [Mg 11]	0.89			
	$MgFe_2O_4$	1000 (*in situ*)	0.8; [Mg 20]	0.80		Thermodyn. model & thermopower	Nell *et al* (1989)
MnFe	$MnFe_2O_4$	1000 then 1300	0.28; [Mn 72]	0.28	∼8.445	Powder XRD	Abbas *et al* (1992)
		700	0.54; [Mn 46]	0.54	8.511	Fe, Mn EXAFS	Yang *et al* (2004)
NiFe	$Ni_{0.93}Fe_{2.07}O_4$	1000	1.0; [Ni 0]	0.93		XANES	Saito *et al* (1999)
	$NiFe_2O_4$	?	∼1.0; [Ni ∼0]	∼1.0		Mössbauer	Šepelák *et al* (2000)
	$NiFe_2O_4$	1400	1.0; [Ni 0]	1.0	8.338	EXAFS	Yao *et al* (1991)
CoFe	$CoFe_2O_4$	1300	0.82–0.70; [18–30]		8.393	Fe Mössbauer	De Guire *et al* (1989)
ZnFe	$ZnFe_2O_4$	1000 then 1300	0.28; [Zn 072]	0.28	∼8.445	Powder XRD	Abbas *et al* (1992)
		1200	<0.01; [Zn ∼99]	0.01	8.4599	Powder ND	Schiessll *et al* (1996)
		500	0.02; [Zn 98]	0.1	8.4419	Powder XRD and	O'Neill (1992)
		950	0.19; [Zn 81]	0.19	8.4400	^{57}Fe Mössbauer	
		700	0.11; [Zn 89]	0.11	8.4432	Neutron PD	Kamiyama *et al* (1992)
		500	0.14; [Zn 86]	0.14	8.4372		
		900	'Some' Fe in tetrahedral sites	'Some' Zn in octahedral sites	8.439	Zn K-edge EXAFS	Tanaka *et al* (1998)
ZnCo	$ZnCo_2O_4$	450	0.2 (Co^{3+}); [Zn 79; Co 20]	0.21	8.102	Powder ND	Krezhov and Konstantinov (1993)
NiMn	$NiMn_2O_4$	900	0.10 Mn^{3+}; [Ni 12, Mn^{2+} 39]	0.88 Ni (+ Mn^{3+} 0.34, Mn^{4+} 0.78)	8.3765	Neutron PD, and thermogravimetry	Baudour *et al* (1992)

Table 1. (Continued.)

Sample name	$M^{2+}M_2^{3+}O_4$	Synthesis or annealing temp	i (M^{3+} in [A]); [x^{Me}; % total element in A]	M^{2+} in [B]	Cell edge(Å)	Method	Source
NiZnFe	$Ni_{0.15}Zn_{0.16}Fe_{2.69}$	?	0.84; [Zn 100; Ni 0]	0.15 (Ni 0.15, Zn 0)		Fe, Ni, Zn EXAFS	Harris *et al* (1995); (1996)
	$Ni_{0.5}Zn_{0.5}Fe_{2.0}$	700 and 1350	0.5 [Zn 100, Ni 0]	0.5 (Ni 0.5; Zn 0)	8.39	Fe, Ni, Zn EXAFS and Fe Mössbauer	Albuquerque *et al* (2000)
MnZnFe	$(Mn_{0.5}Zn_{0.5})Fe_2O_4$	1000 then 1300	0.04; [Zn 96; Mn^{2+} 54]	0.091 (Zn 0.048, Mn 0.043)	∼8.475	Powder XRD	Abbas *et al* (1992)
	$(Mn_{0.5}Zn_{0.5})Fe_2O_4$		∼0; [Zn ∼ 100]	∼0		Powder ND, XAS and Mössbauer	Fatemi *et al* (1999)
ZnNiMn	$Zn_{0.75}Ni_{0.65}Mn_{1.60}$	900	0; [Ni 0, Mn^{2+} 23, Zn 80]	0.8 (Ni 0.65, Mn^{2+} 0.15) + (Mn^{3+} 0.40 + Mn^{4+} 0.80)	8.354	Powder XRD and ND	Guillemet-Fritsch *et al* (2000)
Franklinite FRK2	$(Zn_{0.62}Mn_{0.35}Mg_{0.04})(Fe_{1.94}Al_{0.04}Mn_{0.03})O_4$	Natural	0.078 (Al 0.018, Fe 0.060); [Zn 94, Mn 82, Mg 97; Al 9]	0.079 (Zn 0.035, Mn 0.043, Mg 0.001)$^{2+}$ + (Al 0.016, Fe 1.880, Mn 0.024)$^{3+}$	8.4654	Powder XRD, Mössbauer	Lucchesi *et al* (1999)
NiZnMgFe	$Ni_{0.2}Mg_{0.8}Fe_2O_4$		0.44; [Mg 70]	0.44 ($Mg_{0.24}Ni_{0.2}$)	8.376	Powder XRD and Mössbauer	Amer and El Hiti (2001)
	$Ni_{0.2}Mg_{0.4}Zn_{0.4}Fe_2O_4$		0.46; [Zn 87; Mg 32]	0.46 ($Mg_{0.2}Ni_{0.2}Zn_{0.06}$)	8.404		
	$Ni_{0.2}Zn_{0.8}Fe_2O_4$		0.42; [Zn 73]	0.42 ($Ni_{0.2}Zn_{0.22}$)	8.440		
MgAl	$MgAl_2O_4$	1500 then 800	0.22; [Mg 78; Al 11]	0.22	8.0836	Powder neutron diffraction (PND)	Redfern *et al* (1999)
		700	0.21; [Mg 79; Al 11]	0.21	8.0834	Al^{27} NMR	Wood *et al* (1986)
		900	0.39; [Mg 61; Al 20]	0.39	8.0855		
		700	0.22; [Mg 78; Al 11]	0.22	8.083	Al^{27} NMR	Millard *et al* (1992)
		1000	0.29; [Mg 71; Al 15]	0.29			
		800?	0.32; [Mg 68; Al 16]	0.32	8.0844	PND (*in situ*)	Peterson *et al* (1991) Nakatsuka *et al* (2004)
		1200 then 700 then 300	0.22; [Mg 78; Al 11]	0.11	8.086	Single crystal XRD and ^{27}Al NMR	
		1000 (*in situ*)	0.44; [Mg 56; Al 22]	0.44		Thermodynamic model	Nell *et al* (1989)

Table 1. (Continued.)

Sample name	$M^{2+}M_2^{3+}O_4$	Synthesis or annealing temp	i (M^{3+} in [A]); [x^{Me}; % total element in A]	M^{2+} in [B]	Cell edge Å	Method	Source
MgAlFe	$Mg_{0.70}Fe_{0.23}Al_{1.97}O_4$	1600	0.438 ($Al_{0.23}Fe_{0.21}$); [Mg 66; Al 12]	0.121	8.0670	Single crystal XRD	Foley *et al* (2001) and Pavese *et al* (1999)
	$Mg_{0.99}Al_{1.92}Fe^{3+}_{0.08}O_4$ (3dis) (annealed natural sample)	1000	0.141 ($Al_{0.126}Fe_{0.015}$); [Mg 86; 7]	0.143	8.0973	Single crystal XRD	Martignano *et al* (2006)
	$Mg_{0.77}Fe^{2+}_{0.23}Fe^{3+}_{0.06}Al_{1.94}$ (annealed natural sample, TS2A)	990	0.242 ($Al_{0.241}Fe^{3+}_{0.001}$); [Mg 70; Al 12]	0.242 ($Mg_{0.233}Fe^{2+}_{0.010}$)	8.110	Single crystal XRD	Della Giusta *et al* (1996)
	$Mg_{0.77}Fe^{2+}_{0.074}Fe^{3+}_{0.110}Al_{1.904}$ (natural sample, FAS1)		0.162 ($Al_{0.116}Fe^{3+}_{0.046}$); [Mg 100; Al 6]	0.162 ($Mg_{0.149}Fe^{2+}_{0.061}$)	8.107	Single crystal XRD	Princivalle *et al* (1999)
	$(Mg_{0.5}Fe^{2+}_{0.5})AlFe^{3+}O_4$	1000 (*in situ*)	0.56 ($Al_{0.16}Fe^{3+}_{0.4}$); [Mg 34; Al 16]	0.56 ($Mg_{0.33}Fe^{2+}_{0.23}$)		Thermopower and thermodynamic model	Nell *et al* (1989)
FeAl	$Fe^{2+}Al_2O_4$	1400 then 1100 then 700	0.14; [Fe^{2+} 76]	0.135	8.145	Neutron powder diffraction	Harrison *et al* (1998)
		1000 (*in situ*)	0.2; [Fe^{2+} 10]	0.2		Thermodynamic model and thermopower	Nell *et al* (1989)
ZnAl	$ZnAl_2O_4$	900	0.01; [Zn 99]	0.01	8.0865	Powder XRD	O'Neill and Dollase (1994)
		1300	0.06; [Zn 94]	0.06	8.0844		
NiAl	$NiAl_2O_4$		0.90–0.85; [Ni 10–15]	0.90–0.85		XAS	Lenglet *et al* (1987)
	$NiAl_2O_4$	1400	0.82; [Ni 18]	0.82	8.05	EXAFS	Yao *et al* (1991)
NiAlFe	$NiAlFeO_4$	1400	0.94; [Ni 6]	0.94	∼8.195	EXAFS	Yao *et al* (1991)

data for ordering in $MgAl_2O_4$ (see, e.g., Wood *et al* 1986). However, the element specific, x-ray absorption spectroscopy technique is an ideal probe for studying chemically complex spinels, as structural data can be obtained for *every* element; it is particularly useful for phases having mixtures of 3d transition elements as both crystal structure and valency information can be obtained for each target element by combining XANES and EXAFS data. However, rather few quantitative K-edge EXAFS studies have been published for spinels (see table 1) and this is presumably because the technique generally provides structural information that is averaged over the different sites that the target element might occupy. However, we will show that EXAFS K-edge spectra can be refined to provide estimates of the site distribution over both tetrahedral and octahedral sites in natural and synthetic ferrite spinels of varying chemical complexity. The samples described have previously been used to study L-edge x-ray magnetic circular dichroism (XMCD) spectra to obtain direct information on the ordering of Fe^{3+} and Fe^{2+} over the octahedral and tetrahedral sites in spinels (Pattrick *et al* 2002, Pearce *et al* 2006). In this paper the K-edge XAS results are used to deduce the overall cation intra-site ordering and to assess the wider applicability of this approach for studying complex spinel solid solutions.

2. Experimental methods

2.1. Sample preparation and analysis

Synthetic samples were prepared by mixing stoichiometric amounts of the appropriate high-purity metal oxides (Fe_2O_3, MgO, NiO, CoO, ZnO and Al_2O_3) and heating in a muffle furnace for the temperatures and times given in table 2. Each sample was reground after 12 h to help to homogenize the reaction mixture. Samples of $MgFe_2O_4$ (denoted MgFe) and ZnFe were crystallized at both 1250 and 1450 °C. The higher temperature was used in order to crystallize more Fe^{2+}-rich samples and the resultant materials were coloured red and black, respectively, consistent with the higher-temperature samples being more reduced. Two samples of natural magnetites and a natural franklinite (Zn and Mn rich) were also studied. All samples were analysed by electron microprobe using a Cameca SX100 in the Williamson Research Centre, University of Manchester, with an operating voltage of 15 keV and a specimen current of 20 nA, and with simple oxides, silicates and pure metal as standards. Counting times of 50 s for peak and background measurements were used and all matrix corrections were carried out with the Cameca PAP routine. Five to ten spot analyses were carried out and all samples were found to be homogeneous, with the synthetic samples being close to the ideal compositions chosen. Mean sample analyses and standard deviations are given in table 3 with the Fe^{2+}/Fe^{3+} contents and atomic formulae calculated on a basis of exact stoichiometry with four oxygens and three cations (Droop 1987). All samples are magnetic except for ZnFe synthesized at 1250 °C (ZnFe1250, see table 2).

Unit-cell parameters were determined using Cu Kα radiation on a Philips PW1060 x-ray diffractometer fitted with a curved-crystal graphite monochromator; each sample was mixed with Si as internal standard. Cell parameters were calculated using the UNITCELL programme of Holland and Redfern (1997) and the values (with standard deviations) are given in table 2.

2.2. XAS measurements

All XAS data were collected at the CLRC Daresbury SRS, operating at 2 GeV with an average current of 150 mA. For the Mg and Al K edges the samples were ground with boron nitride and pressed into flat discs. Data were collected *in vacuo* on the soft x-ray station 3.4 operating

Table 2. Samples studied, synthesis conditions and physical properties.

Sample number	Nominal composition	Provenance or synthesis conditions	Cell parameter (Å) (1 sigma)	Magnetic
M873	Fe_3O_4	Natural magnetite. Marmora mine, Madoc, Canada	8.3979(9)	√
M855	Fe_3O_4	Natural magnetite. Iron Mountain, UT, USA	8.3936(7)	√
M6p and M7p	Fe_3O_4	Hydrothermal; 400 °C, 1000 bars, 3 days	8.3960(7)	√
M3226		Natural franklinite. Franklin Furnace, NJ, USA	8.4588(11)	√
MgFe1250, red	$MgFe_2O_4$	1250 °C; 80 h	8.3887(4)	√
MgFe1450, black	$MgFe_2O_4$	1250 °C; 80 h then 1450 °C; 40 h	8.3894(5)	√
CoFe	$CoFe_2O_4$	1050 °C; 80 h	8.3903(8)	√
NiFe	$NiFe_2O_4$	1050 °C; 80 h	8.3381(7)	√
ZnFe1250, red	$ZnFe_2O_4$	1250 °C; 80 h	8.4392(13)	Non-magnetic
ZnFe1450, black	$ZnFe_2O_4$	1250 °C; 80 h then 1450 °C; 40 h	8.4242(6)	√
(CoZn)Fe	$(Co_{0.5}Zn_{0.5})Fe_2O_4$	1100 °C; 110 h	8.4241(7)	√
(CoNi)Fe	$(Co_{0.5}Ni_{0.5})Fe_2O_4$	1250 °C; 80 h	8.3608(7)	√
(CoMg)Fe	$(Co_{0.5}Mg_{0.5})Fe_2O_4$	1250 °C; 80 h	8.3880(13)	√
(NiMg)Fe	$(Ni_{0.5}Mg_{0.5})Fe_2O_4$	1250 °C; 80 h	8.3636(4)	√
(NiZn)Fe	$(Ni_{0.5}Zn_{0.5})Fe_2O_4$	1100 °C; 110 h	8.3937(7)	√
(CoMg)(FeAl)	$(Co_{0.5}Mg_{0.5})FeAlO_4$	1250 °C; 80 h then 1450 °C; 40 h	8.2499(9)	√

Table 3. Electron microprobe analyses (averages of five to ten analyses) of ferrite spinels with Fe^{2+} and Fe^{3+} values calculated for four oxygens and three cations (Droop 1987).

Wt%	M.873	M.855[c]	MT7P	MgFe 1250	MgFe 1450	CoFe	NiFe	ZnFe 1250	ZnFe 1450	Franklinite	(Ni, Mg)Fe	(Ni, Co)Fe	(Ni, Zn)Fe	(Co, Mg)Fe	(Co, Zn)Fe	(Co, Mg) –(Al, Fe)
SiO_2	0.11	—	—	—	0.03	0.03	—	—	0.02	—	—	0.02	—	0.08	0.10	0.10
TiO_2		0.40	—	—	0.01	0.013				0.012		0.02		—	—	0.011
Al_2O_3		0.13	—	—	—	—				0.69						27.4
Cr_2O_3		—	—	—	0.01	—										0.007
Fe_2O_3	70.0	68.0	69.8	78.4	78.6	67.2	66.6	65.1	66.0	66.7	73.6	67.7	66.3	72.5	66.0	41.6
FeO	30.4	29.9	31.4	2.0	2.5	0.15	0.40	0.47	9.9	5.4	1.4	3.1	0.30	0.57	0.43	1.43
MnO	0.13	0.10	—	0.16	0.16	0.007	—	0.12	0.15	9.9	0.14	0.13	—	0.14	—	0.08
MgO	0.36	0.79	—	18.6	18.2	0.005	0.05	0.062	0.069	0.29	9.0	0.06	—	8.9	—	10.1
CoO	—	—	—	—	0.014	31.4	0.37	0.012	0.007	—	—	14.4	0.03	16.9	14.5	19.5
NiO	—	0.04	—	0.02	0.20	0.08	30.2	0.017	0.021	0.012	16.2	13.9	14.9	0.07		0.13
ZnO	—	0.04	—	0.02	0.26	0.011	0.04	32.4	22.1	15.0	—	0.02	17.2	0.015	17.7	0.063
Total	101.0	99.4	101.3	99.1	100.0	98.9	97.6	98.2	98.3	98.0	100.3	99.4	98.6	99.1	98.8	100.4

Table 3. (Continued.)

Wt%	M.873	M.855[c]	MT7P	MgFe 1250	MgFe 1450	CoFe	NiFe	ZnFe 1250	ZnFe 1450	Franklinite	(Ni, Mg)Fe	(Ni, Co)Fe	(Ni, Zn)Fe	(Co, Mg)Fe	(Co, Zn)Fe	(Co, Mg) –(Al, Fe)
Cations 4O, 3cat											—					
Si	0.004	—		—	0.001	0.001	—	—	0.001		—	0.0007	—	0.003	0.004	0.003
Ti		0.012		—	0.0003	0.0002	—	—		0.0004	—					0.0004
Al		0.006		—	—	—	—	—		0.032	—					1.013
Cr		—		—	—	—	—	—			—					0.0001
Fe^{3+}	1.992	1.967	2.000	2.000	1.997	1.997	2.000	2.000	1.999	1.967	2.000	1.999	2.000	1.994	1.992	0.980
Sum 'X' cations[a]	1.996	1.985	2.000	2.000	1.998	1.998	2.000	2.000	2.000	1.999	2.000	1.999	2.000	1.994	1.996	1.997
Fe^{2+}	0.980	0.961	1.000	0.056	0.070	0.005	0.013	0.016	0.333	0.208	0.042	0.102	0.010	0.017	0.015	0.037
Mg	0.020	0.045		0.938	0.914	0.0003	0.003	0.004	0.004	0.017	0.483	0.003	—	0.483		0.470
Mn	0.004	0.003		0.005	0.0045	0.0002	—	0.004	0.005	0.334	0.004	0.004	—	0.004		0.002
Co	—	—			0.0004	0.993	0.012	0.0004	0.0002		—	0.453	0.001	0.496	0.466	0.489
Ni	—	0.001		0.0005	0.0055	0.002	0.971	0.006	0.0007	0.0004	0.471	0.438	0.480	0.002		0.003
Zn	—	0.001		0.0004	0.0065	0.0003	0.001	0.975	0.658	0.440		0.0006	0.509	0.0004	0.523	0.0014
Sum 'Y' cations[b]	1.004	1.011	1.000	1.000	1.002	1.002	1.000	1.000	1.000	1.001	1.000	1.001	1.000	1.006	1.004	1.003

[a] 'X' cations: Fe^{3+}, Al, Cr, Ti, Si.
[b] 'Y' cations: Fe^{2+}, Mg, Mn, Co, Ni, Zn.
[c] Includes 0.13 wt% V_2O_3 and 0.004 V pfu.

in total electron yield and/or fluorescence mode. Spectra at the Mn, Fe, Co, Ni and Zn K-edges were collected in transmission on stations 7.1 and 9.2, with the samples mounted in aluminium sample holders with Sellotape windows and diluted with boron nitride to optimize the edge jump. Data on 7.1 were measured using a vertically collimating plane mirror and a Si(111) double-crystal monochromator detuned to 70% transmission to minimize harmonic contamination. Data on 9.2 were collected using a double-crystal Si(220) monochromator, detuned to 50% transmission. All data were collected at ambient temperature. Energy scales were calibrated using metal foils.

Background subtracted EXAFS spectra were analysed in EXCURV98 using full curved wave theory (Binsted 1998, Gurman *et al* 1984). Phase-shifts were derived in the program from *ab initio* calculations using Hedin–Lundqvist potentials and von Barth ground states (Hedin and Lundqvist 1969). For each refinement a model was set up based on the known crystal structure of magnetite (Fleet 1981), with shells of scatterers based on tetrahedral and octahedral sites. In order to determine the effect of multiple-scattering effects (Gurman *et al* 1986) on the fits, an end member magnetite (sample 873) was refined firstly using single scattering only, then including full cluster multiple scattering from the two sites. The proportion of iron in each site was fixed at 67% octahedral and 33% tetrahedral, and for the multiple scattering the geometry was defined from the crystal structure (Fleet 1981). In order to simplify the calculations only those scatterers within 4 Å of the central metal sites were included. The results for the multiple-scattering model showed no significant improvement of the statistics of the fit compared to that for the single-scattering model and the refined bond-lengths and Debye–Waller factors were within error. It is clear that inclusion of multiple scattering does not have a significant effect on the inner shell parameters of the best fit, therefore only single scattering was used to analyse the data.

3. Results and discussion

3.1. Chemical analyses

The electron microprobe analyses (table 3) have been recalculated assuming stoichiometry (four oxygens and three cations, Droop 1987); the atomic formula unit data including 'model' Fe^{3+} and Fe^{2+} values are also shown in table 3. Note that, except for natural M855 and synthetic (Mg, Co)(Al, Fe), all the samples have Fe^{3+} values close to 2.0 atoms per formula unit (pfu). The hydrothermally synthesized sample (MT7p) is chemically pure and shows exact stoichiometry with a Fe^{3+}/Fe^{2+} ratio of 2.000. Natural magnetite M873 has small concentrations of cations other than Fe but the calculated proportions of Fe^{3+} and Fe^{2+} are very close to stoichiometric ($Fe^{3+}/Fe^{2+} = 2.03$). M855 has quite high Mg contents and Fe^{3+}/Fe^{2+} 2.05. The natural franklinite sample (M3226) is characteristically rich in Zn and Mn, with a very high Fe^{3+}/Fe^{2+} ratio of 9.5, reflecting the substitution of Zn^{2+} and Mn^{2+} for Fe^{2+}.

The stoichiometric calculation method used shows that, even though the synthetic samples were prepared in air, all contain some Fe^{2+} (table 3). The MgFe sample synthesized at 1450 °C (MgFe1450), surprisingly, has only slightly larger Fe^{2+} content than that crystallized at 1250 °C (MgFe1250), but ZnFe1450 has the expected much higher Fe^{2+} compared to ZnFe1250. Note that Zn1450 is ferrimagnetic but ZnFe1250 is non-magnetic, reflecting their different Fe^{3+}–Fe^{2+} stoichiometries. As expected, all of the synthetic samples have very high Fe^{3+}/Fe^{2+} ratios because of the large amounts of Mg, Co, Ni and Zn replacing Fe^{2+}. Sample (Co, Mg)(Fe, Al) is the only synthetic sample with another cation (Al) substituted for Fe^{3+}, and its composition is close to a 50:50 stoichiometric solid solution between the $MgAl_2O_4$ and $CoFe_2O_4$ end

members. Except for M855, all the samples have sums of M^{2+} cations (Y in table 3) very close to 1.000 and, as expected, this is balanced by the sums of $M^{3+} + M^{4+}$ cations being very close to 2.000.

3.2. Refined EXAFS data and site occupancy deductions

The simplest approach when fitting EXAFS data is to refine the spectrum using 'model' structures to obtain mean values for metal–O distances, coordination numbers and Debye–Waller factors for the target element(s). Where the samples are crystalline and of known atomic structure, the quality of the model used is reliable, allowing well defined shells of atoms around the target element to be calculated, and coordination numbers can be assigned to each atomic site. Inspection of a single-crystal, x-ray structure of magnetite (Fleet 1981) shows that the refined EXAFS data should have first shell peaks at ∼1.8 and ∼2.0 Å, corresponding to scattering from oxygens around tetrahedral and octahedral Fe sites, respectively. The next peak at ∼3 Å is due to scattering from metals around the octahedral site *only*, while the peak at ∼3.5 Å includes contributions from metal scatterers around *both* octahedral and tetrahedral sites. The numbers of scatterers in each shell is determined by the proportion of the central metal in each site. We have, therefore, refined our EXAFS data for end-member magnetites M873, M855 and MT6p (tables 2 and 3) on the basis of this structural model as follows.

For each spectrum, the proportion of Fe in each site was refined as a single parameter, together with the absorber–scatterer distances, the Debye–Waller factors and the Fermi energy correction, to minimize a least-squares residual (the *R*-factor (Binsted *et al* 1992)). For example, if the proportion of metal in the tetrahedral site is t, then the proportion of metal in the octahedral site is $(1 - t)$. The number of scatterers (N1) at 1.8 Å (the tetrahedral Met–O distance) would be $4t$ and the number of scatterers (N2) at 2.0 Å (the octahedral Met–O distance) would be $6(1 - t)$. This reduces to $N2 = 6 - 1.5N1$, so by setting this as a constraint and by refining N1 the value of t can be determined. Similarly, the number of scatterers in all the outer shells can also be defined in terms of N1, and these relationships set as constraints. Each outer shell of metal scatterers was modelled as a mixed scatterer site, with the proportion of each metal in the site being determined by the site occupancies given by an initial refinement using an arbitrary mixture, then performing a further refinement to reach the final fit. Our approach differs from those of Yao *et al* (1991) and Wright *et al* (1992) as these authors obtained site occupancies by Fourier filtering and fitting two shells to the first peak in the Fourier transform, while we fitted the whole spectrum without filtering. Note that the third and fourth shells in the FT record the metal–metal interactions, and these make a major contribution to the total EXAFS spectrum.

To test the method the three end-member magnetite samples (table 3) were chosen, and the proportion of iron in each site refined. The refined values are 30:70 tet:oct for sample 873, 30:70 for sample 855, and 33:67 for sample M6P; the ideal proportions are 33% tetrahedral and 67% octahedral occupation. Note that the spectra for these samples were very good quality, out to a k-range of 15 $Å^{-1}$, so this represents the best possible scenario. Figure 1 gives the EXAFS and Fourier transform plots for sample M873, showing the high quality of the fits and the presence of outer-shell peaks at ∼3.0 Å (octahedral Fe only) and ∼3.5 Å (both tetrahedral and octahedral Fe). The refined EXAFS bond lengths and Debye–Waller factor parameters for magnetite M873 are given in table 4 and show excellent agreement with the crystallographic data of Fleet (1981). Table 5 contains other relevant data for all three magnetites including pre-edge peak intensities, edge positions, tetrahedral and octahedral site mean bond lengths and fitted site-occupancy data. Stoichiometric end-member magnetite is believed to contain only Fe^{3+} in tetrahedral coordination (see, e.g., Goodenough and Loeb 1955, Pattrick *et al* 2002), so

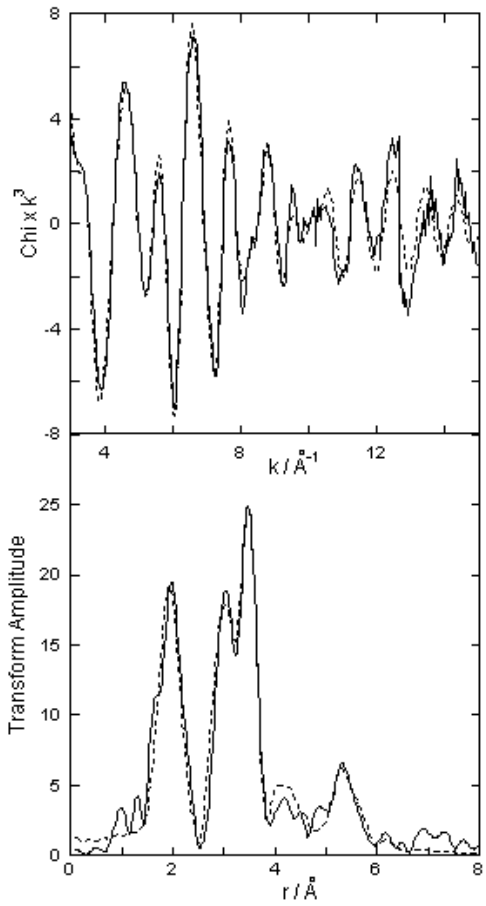

Figure 1. Fe K-edge EXAFS (top) and associated Fourier transform of magnetite M873. Solid lines are the experimental data and the broken lines the best fit.

this Fe^{3+}–O distance can be assigned a value of 1.89 Å, while the octahedral site contains equal numbers of Fe^{3+} and Fe^{2+}, giving a mean EXAFS value of 2.05 Å (table 5). Henderson *et al* (1995) used Fe silicates to assign 'standard' bond lengths of 2.12 Å to $Fe^{2+}_{[VI]}$–O and 2.02 Å to $Fe^{3+}_{[VI]}$–O, giving a mean 50:50 value of 2.07 Å, in good agreement with the mean EXAFS value determined for magnetites and the crystallographic value of 2.058 Å.

The same approach was then used to refine the other target elements in the full sample set. Figure 2 shows a representative EXAFS and FT spectrum for each element. As expected, the data for Mg and Al (soft x-ray energies) are of a lower quality and have shorter data ranges than those for the 3d elements, which will lead to less reliable data, especially for the calculated site occupancies. Table 5 summarizes the data for all the elements in all the samples. Figure 3 allows comparison of the Fe K-edge FT spectra for magnetite with those for the binary ferrites studied (MgFe, NiFe, CoFe, ZnFe), where the varying intensities for the peaks at 3.0 and 3.5 Å give an immediate first-order impression of the octahedral:tetrahedral site occupancies for Fe in the different samples.

Before considering the reliability of the mean M–O bond lengths, we will discuss the site occupancies determined for each divalent element in turn (table 5) in order of decreasing

Table 4. EXAFS structural data obtained on natural magnetite (M873) compared with x-ray, single-crystal structure data.

	Crystal structure (Fleet 1981)				EXAFS fit (single scattering; omitting O shells beyond 4 Å)			
	Tetrahedral site		Octahedral site					
Atom	N	r (Å)	N	r (Å)	N	r (Å)	$2\sigma^2$ (Å^2)	R-factor
O	4	1.889	—	—	1.33	1.90	0.008	30.2
O	—	—	6	2.058	4	2.05	0.004	
Fe	—	—	6	2.968	4	2.99	0.026	
Fe	12	3.480	6	3.480	8	3.49	0.022	
O	12	3.493	—	—	4	3.44	0.024	
Fe	4	3.635	—	—	1.33	3.69	0.015	
O	—	—	8	3.563–3.659	5.33	3.78	0.020	
O	12	4.712	24	4.675–4.748				
Fe	—	—	12	5.140	8	5.21	0.032	
O	12	5.397	—	—				
Fe	16	5.452	8	5.452	10.67	5.50	0.020	
O	4	5.523	—	—				
Fe	12	5.935	12	5.935	12	6.18	0.051	

tendency to occupy tetrahedral sites (the A site) (i.e. tendency to form normal spinel structures). In four synthetic samples and in natural franklinite, 82–90% of the total Zn orders into the tetrahedral site, with the remainder, of course, entering the octahedral site (table 5). In franklinite only 52% of Mn enters the A site (i.e. much smaller proportions than Zn), and in five synthetic, Al-free, ferrite samples 35–50% of Mg enters the A site. By contrast, the (Mg, Co)(Al, Fe) sample has 65% Mg and the pure $MgAl_2O_4$ spinel has 76% of total Mg in the A site; it seems that Al-rich samples show an increasing tendency for Mg to order into A sites to form normal spinels.

In five synthetic ferrites 16–41% and 9–15%, respectively, of the total Co and Ni order into A sites. Although the (Co, Ni)Fe sample shows the same site occupancy for both Co and Ni (table 5), it seems that, overall, Ni shows the greater tendency to form the inverse structure type, in line with the fact that Ni has a larger octahedral site preference energy than Co (Burns 1993). We have also obtained occupancy data for Al in $MgAl_2O_4$ spinel and one Fe–Al-rich synthetic sample (table 5), and both show the same result of 10% of the bulk Al entering the A site.

In all cases, we assume that all the Fe occupying the tetrahedral site is present as Fe^{3+}. For the full range of synthetic ferrite samples and natural franklinite, the occupancy of Fe^{3+} in the A site varies from a maximum of 52% to a minimum of 10% of the total Fe (equivalent to A site occupancies varying from ∼0.92 to ∼0.19), reflecting that the normal or inverse character of ferrite spinels is mainly controlled by the crystal chemical properties of the other cations present.

The A-site occupancy data derived from EXAFS have also been combined with the electron microprobe data to calculate mass balance data for the tetrahedral site, and the results are given in table 5 as cations pfu. The tetrahedral cation sums for the ferrites are rather high, ranging from 1.02 to 1.23 (averaging 1.12 ± 0.06), but there is no evidence that the data for any one element are less reliable than for any other. It seems that the method tends to give slightly high occupancy factors for the A-sites, and we have normalized our measured values to a total of 1.0 atom pfu for this site (table 5). Bearing in mind the uncertainties in this approach to

Table 5. XANES and EXAFS information for natural and synthetic spinels.

					Tetrahedral			Octahedral	
Sample	Edge	Pre-edge eV[a]	Edge eV[b]	Pre-edge/ edge	%	r (Å)	Occupancy atoms pfu (normalized occupancy)	%	r (Å)
Magnetite 873	Fe K	7113.9	7123.1	0.052	33	1.90		67	2.05
Magnetite 855	Fe K	7114.0	7123.8	0.046	33	1.89		67	2.03
Magnetite M6P	Fe K	7113.9	7123.5	0.051	33	1.88		67	2.05
Magnetite,	Fe K	7113.7	7125.7	0.037	27	1.77	0.587 (0.518)	73	2.01
Franklin 3266	Mn K				52	1.88	0.174 (0.154)	48	2.00
	Zn K				82	1.97	0.361 (0.318)	18	2.15
$CoFe_2O_4$	Fe K	7113.9	7125.2	0.062	35	1.78	0.701 (0.636)	65	1.96
	Co K		7716.3		41	1.92	0.401 (0.364)	59	2.07
$NiFe_2O_4$	Fe K	7114.0	7125.4	0.058	52	1.80	1.047 (0.923)	48	1.94
	Ni K		8336.5		9	1.86	0.087 (0.077)	91	2.05
$MgFe_2O_4$,	Fe K	7114.0	7125.7	0.066	33	1.79	0.678 (0.591)	67	1.97
1250 °C, red	Mg K				50	1.98	0.469 (0.409)	50	2.07
$MgFe_2O_4$,	Fe K	7114.0	7125.8	0.065	33	1.78	0.682 (0.624)	67	1.97
1450 °C, black	Mg K				45	1.98	0.411 (0.376)	55	2.09
$ZnFe_2O_4$,	Fe K	7114.0	7124.6	0.028	10	1.72	0.202 (0.187)	90	2.01
1250 °C, red	Zn K				90	1.95	0.876 (0.813)	10	2.09
$ZnFe_2O_4$,	Fe K	7113.9	7125.4	0.026	20	1.71	0.466 (0.441)	80	2.00
1450 °C, black	Zn K				90	1.95	0.592 (0.559)	10	2.12
$Co_{0.5}Ni_{0.5}Fe_2O_4$	Fe K	7113.9	7125.2	0.065	45	1.79	0.945 (0.873)	55	1.95
	Co K		7715.9		16	1.81	0.072 (0.067)	84	2.05
	Ni K		8336.5		15	1.85	0.066 (0.060)	85	2.05
$Co_{0.5}Zn_{0.5}Fe_2O_4$	Fe K	7114.0	7125.4	0.037	32	1.78	0.642 (0.545)	68	1.99
	Co K		7716.5		22	1.77	0.103 (0.087)	78	2.05
	Zn K				83	1.95	0.434 (0.368)	17	2.05
$Ni_{0.5}Zn_{0.5}Fe_2O_4$	Fe K	7114.0	7125.6	0.041	34	1.79	0.683 (0.582)	66	1.98
	Ni K		8336.4		12	1.84	0.057 (0.049)	88	2.05
	Zn K				85	1.96	0.433 (0.369)	15	2.10
$Co_{0.5}Mg_{0.5}Fe_2O_4$	Fe K	7113.9	7125.7	0.062	45	1.80	0.905 (0.735)	55	1.96
	Co K		7716.2		22	1.85	0.109 (0.089)	78	2.05
	Mg K				45	1.96	0.217 (0.176)	55	2.05
$Ni_{0.5}Mg_{0.5}Fe_2O_4$	Fe K	7113.9	7125.7	0.069	45	1.81	0.919 (0.806)	55	1.96
	Ni K		8336.3		11	1.82	0.052 (0.046)	89	2.04
	Mg K				35	1.95	0.169 (0.148)	65	2.05
$Co_{0.5}Mg_{0.5}$–	Fe K	7114.0	7125.8	0.064	45	1.88	0.458 (0.448)	55	1.99
$Fe_{0.5}Al_{0.5}O_4$	Co K		7715.7		30	1.78	0.147 (0.144)	70	2.00
	Mg K				65	1.94	0.306 (0.299)	35	2.09
	Al K				11	1.74	0.111 (0.109)	89	1.90
$MgAl_2O_4$	Mg K				76	1.94	0.760 (0.792)	24	2.17
	Al K				10	1.75	0.240 (0.208)	90	1.91

[a] Pre-edge position ±0.3 eV, defined as centre of pre-edge w.r.t. Fe foil first peak in derivative defined as 7111.1 eV (Wilke *et al* 2001).
[b] Edge position ±0.3 eV, defined as point half way up absorption edge w.r.t. (i) Fe foil first peak in derivative defined as 7111.1 eV; (ii) Co foil first peak in derivative defined as 7706.8 eV; Ni foil first peak in derivative defined as 8327.0 eV.

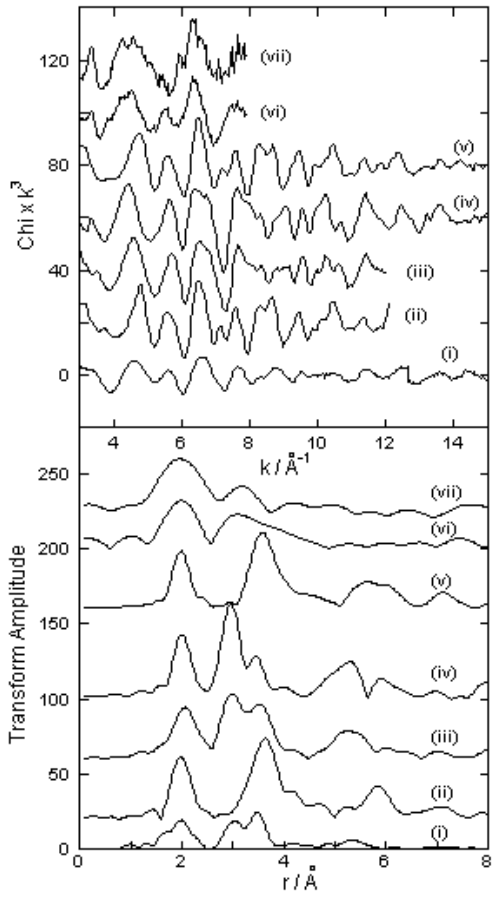

Figure 2. Experimental EXAFS spectra (top) and associated Fourier transforms of (i) Fe K edge in M873, (ii) Mn K edge in franklinite 3226, (iii) Co K edge in $CoFe_2O_4$, (iv) Ni K edge in $NiFe_2O_4$, (v) Zn K edge in $ZnFe_2O_4$ (1250 °C), (vi) Mg K edge in CoMg–FeAl and (vii) Al K edge in CoMg–FeAl.

determining site occupancies, we believe that our data are reliable for a wide range of elements that can enter the ferrite spinel structure.

We have shown that the Fe–O bond lengths determined by EXAFS for the end-member magnetites are close to the expected values. Assuming that all Fe in tetrahedral sites is Fe^{3+}, the data in table 5 show that mean $(Fe^{3+}–O)^A$ distances for all other ferrites are anomalously small, falling in the range 1.71–1.88 Å. The smallest values are for samples with the lowest contents of Fe in tetrahedral sites, pointing to the difficulty of fitting the first M–O shell reliably (see the spectrum for ZnFe in figure 3). However, even samples with significant Fe contents in tetrahedral sites tend to have rather small Fe^{3+}–O distances (e.g. NiFe, table 5), and it is possible that the presence of other cations in the ferrite structure is causing site distortions, as it is well known (Eisenberger and Brown 1979) that EXAFS tends to return small M–O distances for distorted sites. Refinement using second and third cumulant expansions showed no significant improvement. We cannot reliably assess the data for Fe–O distances in octahedral sites because we have no reliable estimate of the Fe^{2+}:Fe^{3+} ratio in this site. However, standard values of $Fe^{2+}_{[VI]}$–O = 2.12 Å and $Fe^{3+}_{[VI]}$–O = 2.02 Å are both larger than the mean EXAFS

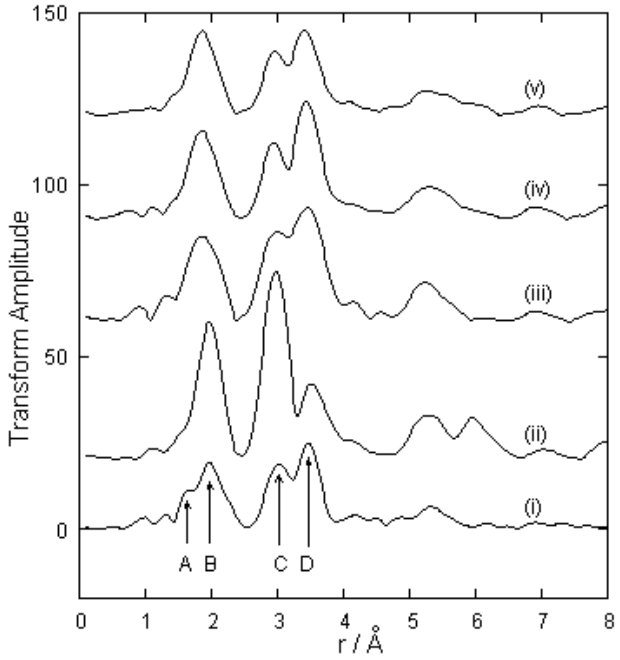

Figure 3. Fe K-edge EXAFS spectra of Fe in (i) magnetite M873, (ii) $ZnFe_2O_4$ (1250 °C), (iii) $CoFe_2O_4$, (iv) $NiFe_2O_4$ and (v) $MgFe_2O_4$ (1250 °C). Feature A is due to oxygens coordinated to iron in the tetrahedral site; B is due to oxygens coordinated to iron in the octahedral site; C is due to the metal–metal distance between neighbouring octahedral sites; D is due to the metal–metal distance between neighbouring octahedral and tetrahedral sites.

Fe–O bond length determined for all the samples (range 1.95–2.01), again suggesting that the EXAFS values are affected by site distortions.

The mean first-shell EXAFS distances determined for the other major cations present in the natural franklinite and synthetic samples are given in table 5 for both the tetrahedral and octahedral sites and can be compared with recommended bond lengths from other published work summarized in table 6. The lower EXAFS bond lengths tend to be for samples with low contents of the element in the appropriate site, although there does seem to be a tendency for the EXAFS bond lengths to be anomalously short (cf table 6, Ni and Co in the octahedral and Mn in the tetrahedral site), perhaps due to site distortions as discussed for Fe above.

3.3. Comparison to published data for spinels

Our data in table 5 can be compared to representative published results summarized in table 1. For most samples of equivalent stoichiometries, our unit-cell parameters are within 0.005 Å of the published data. However, the published values for $MgFe_2O_4$ show a significant range (8.360–8.400 Å), with our sample falling in the middle (8.389 Å). Our data for the percentage of total Mg occupying the tetrahedral site in MgFe (denoted $x^{Mg} = 50\%$, table 5) is significantly larger than any of the published values for this stoichiometry (range 10–29%, table 1). In published work on NiFe, and other more complex ferrites, all Ni is assigned to the B site ($x^{Ni} = 0\%$) compared with our values (range 9–15%). Our values for x^{Co} (15–41%) are similar to published values (18–30%) and the value for x^{Mn} obtained for the Mn-rich franklinite (52%) lies at the middle of a very wide range published for x^{Mn} (23–88%). Our

Table 6. Published M–O bond-lengths, adopted values and EXAFS data.

	M–$O^{a}_{(IV)}$ (Å)						M–$O^{a}_{(VI)}$ (Å)					
M	1[b]	2	3	4	5	6	1	2	3	4	5	6
Mg	1.95	1.935	1.965	1.96	1.96	1.94–1.98	2.10	2.09	2.095	2.08	2.09	2.07–2.09
Mn^{2+}	2.04	2.035	2.04		2.04	1.88	2.21	2.18			2.21	2.00
Mn^{3+}							2.025				2.025	
Fe^{2+}	2.01	1.995	1.996	2.01			2.16	2.12	2.138	2.13	2.11	
Co	1.96	1.96			1.98[c]	1.77–1.92	2.125	2.10			2.10	2.00–2.07
Ni	1.93	1.945	1.974		1.96	1.80–1.85	2.07	2.07	2.076		2.065	2.03–2.05
Zn	1.98	1.96	1.966		1.975[d]	1.95–1.96	2.12	2.11			2.12	2.05–2.12
Al	1.77	1.77	1.767	1.77	1.77	1.74–1.75	1.915	1.91	1.909	1.91	1.91	1.90–1.91
Fe^{3+}	1.87	1.865	1.891	1.89	1.88	1.72–1.88	2.025	2.025	2.020	2.00	2.01	1.94–2.01
Si	1.64	1.655		1.65	1.65		1.78			1.79	1.79	
Ti	1.80	1.80		1.80	1.80		1.985	1.98		1.98	1.98	

[a] O = 1.38 Å.
[b] 1, Shannon 1976; 2, O'Neill and Navrotsky (1983); 3, Della Giusta *et al* (1996); 4, Hazen and Yang (1999); 5, adopted values; 6, EXAFS data.
[c] Henderson *et al* (1997).
[d] Takes account of 1.999 Å (Lucchesi *et al* 1999).

x^{Zn} values (82–90%) are similar to the lower end of published data for $ZnFe_2O_4$ (72–90%), but note that for published data on chemically more-complex ferrites effectively all Zn was assigned to the A site ($x^{Zn} = 100\%$). The published work shows that x values for Zn, Mg and Ni are all larger for end-member aluminate spinels than for the equivalent Fe end-member ferrites (table 5), and our data for MgFe, (Mg, Co)(Al, Fe) and MgAl confirm this trend for x^{Mg} (values of 50, 65, 76% respectively). The equivalent x^{Al} for these last two samples (11 and 10% respectively) are within the published range for aluminous spinels (6–22%). Although there are many similarities for most elements between our data and the published results, we believe that our data set is generally better defined, especially for chemically more complex samples. We will return to this point later.

3.4. Metal valencies from XANES spectra

It is well known that the position and intensity of the 1s–3d pre-edge peak and refined first-shell M–O bond distances in Fe K-edge XAS spectra can be used to assess the valencies and coordination of Fe in crystalline and amorphous phases (see, e.g., Waychunas *et al* 1983, Henderson *et al* 1995, Wilke *et al* 2001, Berry *et al* 2003). Henderson *et al* (1995) assigned 'standard' values for pre-edge intensities relative to the step height of $Fe^{2+}_{[IV]}$ 0.05, $Fe^{2+}_{[VI]}$ 0.02, $Fe^{3+}_{[IV]}$ 0.12 and $Fe^{3+}_{[VI]}$ 0.02, but since then Wilke *et al* (2001) and Berry *et al* (2003) have greatly improved this type of analysis by relating pre-edge peak areas and energies to varying oxidation ratios. Although pre-edge heights and energies for the ferrite sample K edges are given in table 5, the resolution of the XANES spectra is not adequate to make meaningful comparisons to the results of Wilke *et al* (2001). Nevertheless, the main control of pre-edge peak intensity in these samples is the amount of Fe^{3+} in tetrahedral coordination, as both Fe^{3+} and Fe^{2+} have similar and smaller pre-edge peak intensities for octahedral coordination. We would therefore expect to see a coupled relationship between pre-edge peak size for our samples and the percentage of the total Fe occupying tetrahedral sites as Fe^{3+}. Figure 4 shows a well defined trend for these variables and it seems that the pre-edge data are in reasonable agreement with the site occupancies for Fe^{3+} determined from the EXAFS data.

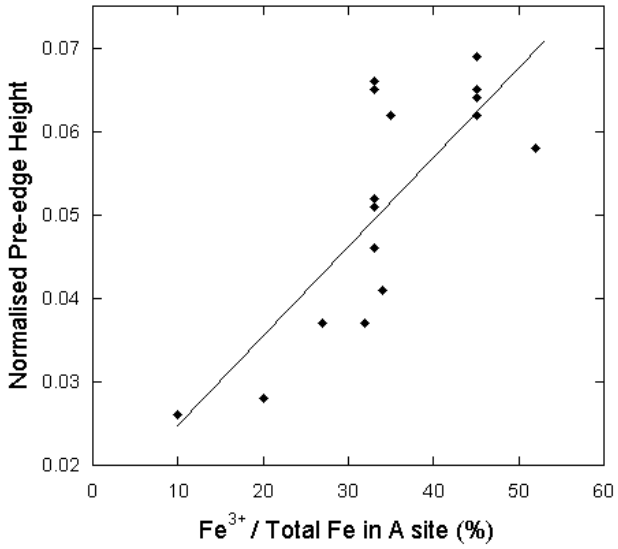

Figure 4. Relationship between the Fe pre-edge height (normalized to the edge height) and the percentage of Fe present as Fe^{3+} in the A site (tetrahedral). The line provides a 'guide to the eye'.

The K-edge position for Ni in NiFe is within the error of that for NiO (8336.5 and 8336.1 eV, respectively), and their XANES features are very similar in shape and intensity. The Co edge position in CoFe is very close to that for CoO (7716.3 and 7716.0 eV) and their XANES spectra are also similar. These features point to the presence of only Ni^{2+} and Co^{2+} in the synthetic ferrites.

3.5. Unit-cell parameters and site occupancy data

The oxide spinels have cubic symmetry (space group *Fd3m*) and the unit-cell geometry is controlled by only the metal–oxygen bond lengths for the tetrahedral (A–O) and octahedral (B–O) sites (Hill *et al* 1979). The unit-cell edge (a) and oxygen parameter (u, the displacement of O from the atomic coordinate 0.25) are related to these two distances by the following equations:

$$a = (8/11\sqrt{3})[5(\text{A–O}) + \sqrt{33}(\text{B–O})^2 - 8(\text{A–O})^2]$$

$$u = (0.75R - 2 + \sqrt{(33R/16 - 0.5)})/[6(R-1)] \qquad \text{where } R = (\text{B–O})^2/(\text{A–O})^2.$$

The ordering arrangements of different sized cations over the tetrahedral and octahedral sites clearly control the values for a and u. Because it is straightforward to obtain high precision values for a, it is possible to use these values to test the general reliability of the measured site occupancy data for each major cation in our sample set, but reliable metal–O bond lengths must be assigned for each appropriate valency and cation site. Note that in our synthetic ferrites only Fe occurs in two valency states, with Fe^{3+} as the dominant species, and this simplifies the crystal chemical modelling.

The structure of end-member magnetite (Fleet 1981) gives bond lengths $(Fe^{3+}\text{–O})^{T} = 1.889$ Å and $(\text{Fe–O})^{M} = 2.058$ Å, where $(\text{Fe–O})^{M}$ is the mean distance for one atom each of 'nominal' Fe^{2+} and Fe^{3+}. We have assigned a bond length of 2.01 Å to $(Fe^{3+}\text{–O})^{M}$, in line with reasonable published values (table 6), which leads to a value of 2.11 for $(Fe^{2+}\text{–O})^{M}$ (i.e. a mean value of 2.06 for magnetite). An internally consistent set of bond-length data for the other

Table 7a. Measured and derived parameters for binary synthetic spinels for stoichiometry AB_2O_4.

Parameter	MgFe1250	CoFe	NiFe	ZnFe1250	MgAl
Measured a (Å)	8.3887	8.3903	8.3381	8.4392	8.0804(12)[c]
Measured A site occupancy of 2+ cation for $T_{total} = 1.0$ atom pfu	Mg 0.41	Co 0.36	Ni 0.08	Zn 0.81	Mg 0.79
(total 2+ cation in sample pfu)	(Mg 0.94)	(Co 0.99)	(Ni 0.97)	(Zn 0.98)	(Mg 1.0)
Calculated occupancy of 2+ cation in A for proportion of total Fe as Fe^{2+} in B site:					
0%	TS[a]	0.7	0.3	TS	0.7
5–10%	TS–0.9	0.35–0.10	0.15–0	TS–TS	
15–20%	0.5–0.2	TL–TL	TL–TL	TS–0.65	
25–30%	0.05–TL[b]	TL–TL	TL–TL	0.2–TL	
Parameters calculated from measured site occupancies					
Mean A–O (Å)	1.913	1.909	1.887	1.957	1.903
Mean B–O (Å)	2.042	2.046	2.038	2.038	1.937
a (Å)	8.386	8.391	8.337	8.440	8.084
u	0.2567	0.2563	0.2557	0.2589	0.2609
Calculated (Fe^{2+}/total Fe) for B site	0.15	0.10	0.070	0.20	—
XMCD (Fe^{2+}/total Fe) for B site	0.16	0.11	0.15	—	—
Recommended factors for tetrahedral site occupancies	Mg [average of 5] (1 sigma std dev)	Co [5]	Ni [4]	Zn [4]	Mg [1]; Al [1]
Ferrites	0.44 (0.12)	0.24 (0.09)	0.11 (0.02)	0.76 (0.06)	
Aluminous spinel					0.79; 0.21
Ferrites	Mn (franklinite) 0.45	Al [(Co, Mg)(Fe, Al)] 0.11			

[a] TS = calculated cell parameter too small for full occupancy range to match measured value.
[b] TL = too large.
[c] Henderson and Taylor (1975).

Table 7b. Measured and derived parameters for synthetic spinels and natural franklinite.

Parameter	(Ni, Mg)Fe	(Ni, Co)Fe	(Ni, Zn)Fe	(Co, Mg)Fe	(Co, Zn) Fe	(Co, Mg)(Fe, Al)	MgFe 1450	ZnFe 1450	Franklinite
Measured a (Å)	8.3636	8.3608	8.3937	8.3880	8.4241	8.2499	8.3894	8.4242	8.4588
Measured A site occupancy of 2+	Ni 0.05	Ni 0.06	Ni 0.05	Co 0.09	Co 0.09	Co 0.14 (0.489)	Mg 0.38	Zn 0.56	Zn 0.32
cation for $T_{\text{total}} = 1.0$ atom pfu	(0.471)	(0.438)	(0.4800)	(0.496)	(0.466)	Mg 0.30 (0.470)	(0.914)	(0.66)	(0.440)
(total 2+ cation in sample pfu)	Mg 0.15	Co 0.07	Zn 0.37	Mg 0.18	Zn 0.37	Fe 0.44 (1.02)			Mn 0.15
	(0.483)	(0.453)	(0.509)	(0.483)	(0.523)	Al 0.11 (1.01)			(0.334)
Calculated parameters for measured cation occupancies for all significant elements									
Mean A–O (Å)	1.896	1.892	1.919	1.907	1.924	1.908	1.911	1.933	1.935
Mean B–O (Å)	2.043	2.044	2.041	2.046	2.049	1.995	2.044	2.045	2.056
a (Å)	8.364	8.361	8.393	8.388	8.422	8.251	8.389	8.424	8.457
u	0.2559	0.2557	0.2570	0.2563	0.2569	0.2585	0.2565	0.2575	0.2571
Calculated (Fe^{2+}/total Fe) for B	0.13	0.11	0.17	0.11	0.20	0.25	0.17	0.42	0.34
XMCD (Fe^{2+}/total Fe) for B	0.12	0.13	0.13	0.14	0.12	0.20	—	0.29	0.28

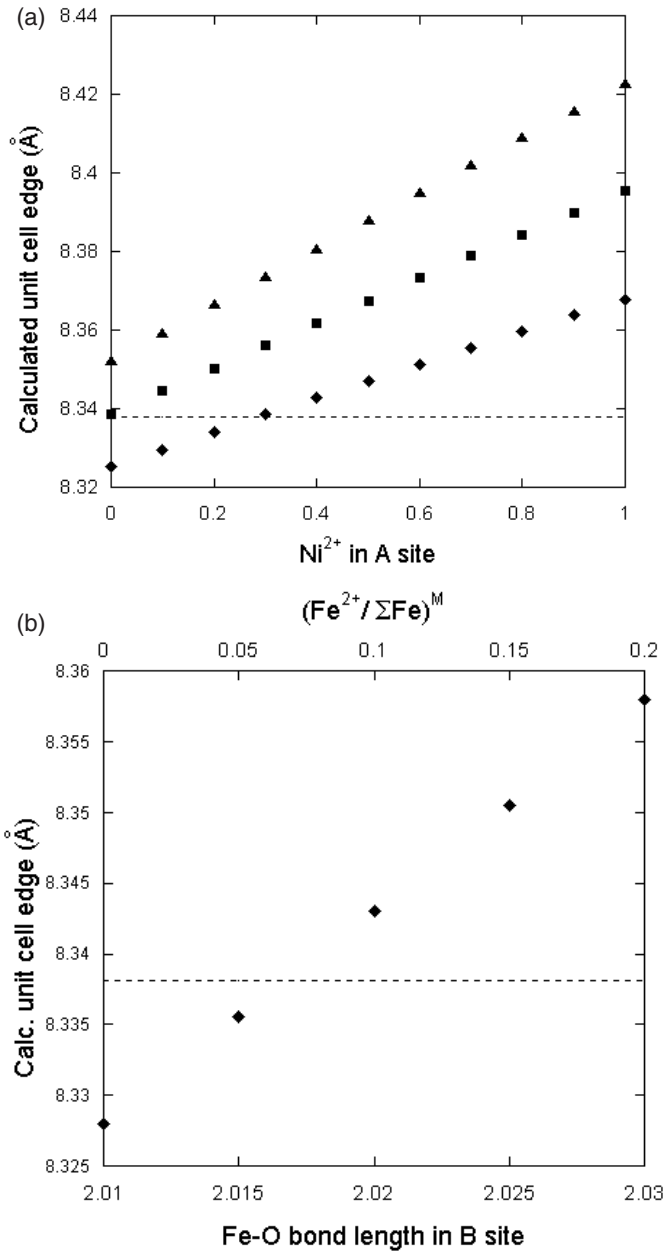

Figure 5. (a) Calculated unit-cell edge for NiFe with zero (diamonds), 10% (squares) and 20% (triangles) Fe^{2+} in the B site ($(Fe–O)^B$ = 2.01, 2.02 and 2.03 Å, respectively). The dotted line shows the measured unit-cell edge of 8.3381 Å. (b) Calculated unit-cell edge for NiFe as a function of the Fe–O bond length in the B site (bottom *x*-axis).

cations is given in table 6, and these can be applied to our synthetic binary ferrites and spinel (*ss*) to confirm the reliability of the measured tetrahedral occupancy factors. The calculated *a* is sensitively dependent on the bond lengths used and, based on our full data set, it was found that the published data for $(Co–O)^A$ give low calculated *a* values and those for $(Ni–O)^B$ give

an a value that is too high. Values chosen, therefore, are 1.98 Å (Henderson *et al* 1997) and 1.975 Å, respectively. Note also that the value used for $(Zn–O)^A$ (1.75 Å) lies midway in the wide range reported in the literature (1.96–1.999 Å, table 6).

We summarize our approach using the data for NiFe as this is the most ordered of all our samples. A spreadsheet was set up to calculate the A–O and B–O bond lengths and cell edge, a, for all A site occupancies from zero to unity, and the calculated a value was compared to the measured value. It was found that an $(Fe^{3+}–O)^A$ value of 1.89 Å gave a values larger than the measured value for all A-site occupancy factors (e.g., for 0.0 Ni occupancy $a = 8.340$ Å compared to the measured value of 8.338 Å). The CoFe sample gave a similar result, and as the presence of some Fe^{2+} in the B site (Pattrick *et al* 2002) would give even larger a values (bigger mismatches with the measured a), a bond length of 1.88 Å for $(Fe–O)^A$ was adopted for all the remaining calculations. Figure 5(a) includes model calculations for NiFe with zero, 10% and 20% Fe^{2+} in the B site ($(Fe–O)^B = 2.01$, 2.02 and 2.03 Å, respectively) and shows that the measured a can be matched with between 5 and 10% of the B site as Fe^{2+} (cf figure 5(b)). Model results for all the binary spinels are given in table 7a, with data shown for $(Fe–O)^B$ from 2.01 to 2.03 Å, equivalent to Fe^{2+} contents in the B site of 0–0.2 atoms pfu. The calculated occupancy factor for MgAl shows good agreement with the measured values, as do the values calculated for NiFe and CoFe for Fe^{2+} in the range of 0.05–0.10 atoms pfu. However, MgFe1250 and ZnFe1250 only show good agreement for the calculated and measured occupancy factors for larger Fe^{2+} contents of 0.15 and 0.20, respectively (table 7a).

The *measured* occupancy factors and microprobe analyses for all the samples were then combined to calculate cell parameters, oxygen parameters and approximate Fe^{2+} contents, and the results are given in tables 7a and 7b. For most samples the calculated Fe^{2+}/total Fe in the B site and that measured by XMCD are very similar, although for the most reduced samples, Zn1450 and franklinite, the calculated values are about 25% higher than the XMCD values (tables 7a and 7b). Considering the various uncertainties and the range of chemical compositions, the results for the different samples are internally consistent. We therefore suggest that the values we have adopted for tetrahedral and octahedral M–O bond lengths (table 6) and the mean tetrahedral occupancy factors determined for each element (table 7a) are the best estimates available for this suite of elements in ferrite spinels and provide an internally consistent data set for crystal chemical treatment of this structure type. Thus the order of increasing tendency to order into tetrahedral sites in ferrites is $Fe^{2+} < Ni < Al < Co < Mg = Mn < Zn$. The tetrahedral occupancy factor for Fe^{3+} covers a wide range (0.92–0.19), suggesting that Fe^{3+} plays a relatively passive role and merely makes good any deficit in the A site.

Acknowledgments

We thank Professor Richard Pattrick for collecting EXAFS data for the $NiFe_2O_4$ sample and Dr Carolyn Pearce for providing information on the XMCD results for the (Co, Mg)(Al, Fe) sample.

References

Abbas T, Khan Y, Ahmad M and Anwar S 1992 X-ray diffraction study of the cation distribution in the Mn–Fe-ferrites *Solid State Commun.* **82** 701–3

Albuquerque A, Ardisson J D and Macedo W A A 2000 Nanosized powders of NiZn ferrite: synthesis, structure and magnetism *J. Appl. Phys.* **87** 4352–7

Amer M A and El Hiti M 2001 Mössbauer and x-ray studies for $Ni_{0.2}Zn_xMg_{0.8-x}Fe_2O_4$ ferrites *J. Magn. Magn. Mater.* **234** 118–25

Baudour J L, Bouree F, Fremy M A, Legros R, Rousset A and Gillot B 1992 Cation distribution and oxidation states in nickel manganites $NiMn_2O_4$ and $Ni_{0.2}Mn_{2.2}O_4$ from powder neutron diffraction *Physica* B **180/181** 97–9

Berry A J, O'Neill H St C, Jayasuriya K D, Campbell S J and Foran G J 2003 XANES calibrations for the oxidation state of iron in a silicate glass *Am. Mineral.* **88** 967–77

Binsted N 1998 *Daresbury Laboratory EXCURV98 Program*

Binsted N, Strange R W and Hasnain S S 1992 Constrained and restrained refinement in EXAFS data analysis with curved wave theory *Biochemistry* **31** 12117–25

Burns R G 1993 *Mineralogical Applications of Crystal Field Theory* (Cambridge: Cambridge University Press) p 249

Carbonin S, Russo U and Della Giusta A 1996 Cation distribution in some natural spinels from x-ray diffraction and Mössbauer spectroscopy *Mineral. Mag.* **60** 355–68

De Guire M R, O'Handley R C and Kalonji G 1989 The cooling rate dependence of cation distributions in $CoFe_2O_4$ *J. Appl. Phys.* **65** 3167–72

Della Giusta A, Carbonin S and Ottonello G 1996 Temperature-dependent disorder in a natural Mg–Al–Fe^{2+}–Fe^{3+}-spinel *Mineral. Mag.* **60** 603–16

Droop G T R 1987 A general equation for estimating Fe^{3+} concentrations in ferro-magnesian silicates and oxides from microprobe analyses, using stoichiometric criteria *Mineral. Mag.* **51** 431–5

Eisenberger P and Brown G S 1979 The study of disordered systems by EXAFS: limitations *Solid State Commun.* **29** 481–4

Fatemi D J, Harris V G, Chen M X, Malik S K, Yelon W B, Long G J and Mohan A 1999 X-ray absorption, neutron diffraction, and Mössbauer effect studies on MnZn-ferrite processed through high-energy ball milling *J. Appl. Phys.* **85** 5172–4

Fleet M E 1981 The structure of magnetite *Acta Crystallogr.* B **37** 917–20

Foley J A, Wright S E and Hughes J M 2001 Cation partitioning versus temperature in spinel: optimization of site occupants *Phys. Chem. Minerals* **28** 143–9

Frost B R 1991 Stability of oxide minerals in metamorphic rocks *Rev. Mineral. (Min. Soc. Am.)* **25** 469–87

Frost B R and Lindsley D H 1991 Occurrence of iron–titanium oxides in igneous rocks *Rev. Mineral. (Min. Soc. Am.)* **25** 433–68

Goodenough J B and Loeb A L 1955 Theory of ionic ordering, crystal distortion, and magnetic exchange due to covalent forces in spinels *Phys. Rev.* **98** 391–408

Guillemet-Fritsch S, Baudour J L, Chanel C, Bouree F and Rousset A 2000 X-ray and neutron diffraction studies on nickel zinc manganite $Mn_{2.35-x}Ni_{0.65}Zn_xO_4$ powders *Solid State Ion.* **132** 63–9

Gurman S J, Binsted N and Ross I 1984 A rapid, exact, curved-wave theory for EXAFS calculations *J. Phys. C: Solid State Phys.* **17** 143–51

Gurman S J, Binsted N and Ross I 1986 A rapid, exact, curved-wave theory for EXAFS calculations. 2. The multiple-scattering contributions *J. Phys. C: Solid State Phys.* **19** 1845–61

Harris V G, Koon N C, Williams C M, Zhang Q and Abe M 1996 Cation distribution in NiZn-ferrite films determined using x-ray absorption fine structure *J. Appl. Phys.* **79** 4561–3

Harris V G, Koon N C, Williams C M, Zhang Q, Abe M, Kirkland J P and McKeown D A 1995 Direct measurement of octahedral and tetrahedral environments in NiZn-ferrites *IEEE Trans. Magn.* **31** 3473–5

Harrison R J and Putnis A 1999 Determination of the mechansim of cation ordering in magnesioferrite ($MgFe_2O_4$) from the time-dependence of magnetic susceptibility *Phys. Chem. Minerals* **26** 322–32

Harrison R J, Redfern S A T and O'Neill H St C 1998 The temperature dependence of the cation distribution in synthetic hercynite ($FeAl_2O_4$) from *in situ* neutron refinements *Am. Mineral.* **83** 1092–9

Hazen R M and Yang H 1999 Effects of cation substitution and order-disorder on P–V–T equations of state of cubic spinels *Am. Mineral.* **84** 1956–60

Hedin L and Lundqvist S 1969 Effects of electron–electron and electron–phonon interactions on the one-electron states of solids *Solid State Phys.* **23** 1–181

Henderson C M B, Charnock J M, Cressey G C and Griffen D T 1997 An EXAFS study of Fe, Co, Zn and Mg in natural and synthetic staurolites *Mineral. Mag.* **61** 613–25

Henderson C M B, Cressey G C and Redfern S A T 1995 Geological applications of synchrotron radiation *Radiat. Phys. Chem.* **45** 459–81

Henderson C M B and Taylor D 1975 Thermal expansion by x-ray diffraction: use of specimen holder as internal standard and expansion of MgO (periclase) and $MgAl_2O_4$ (spinel) *Trans. J. Brit. Ceram. Soc.* **74** 55–7

Hill R J, Craig J R and Gibbs G V 1979 Systematics of the spinel structure type *Phys. Chem. Minerals* **4** 317–40

Holland T J B and Redfern S A T 1997 Unit-cell refinement from powder diffraction data: the use of regression diagnostics *Mineral. Mag.* **61** 65–77

Kamiyama T, Haneda K, Sato T, Ikeda S and Asan H 1992 Cation distribution in $ZnFe_2O_4$ fine particles studied by neutron powder diffraction *Solid State Commun.* **81** 563–6

Krezhov K and Konstantinov P 1993 On the cationic distribution in zinc–cobalt oxide spinels *J. Phys.: Condens. Matter* **5** 9287–94

Lenglet M, D'Huysse A, Bonelle J P, Dürr J and Jørgensen C K 1987 Analysis of x-ray NiKβ emission, XANES, XPS, Ni 2p, and optical spectra of nickel (II) spinels and structure inference *Chem. Phys. Lett.* **136** 478–82

Lindsley D H 1976 The crystal chemistry and structure of oxide minerals as exemplified by the Fe–Ti oxides *Oxide Miner. Min. Soc. Am. Short Course Notes* **3** L1-60

Lucchesi S, Russo U and Della Giusta A 1999 Cation distribution in natural Zn-spinels: franklinite *Eur. J. Mineral.* **11** 501–11

Martignano F, Andreozzi G B and Dal Negro A 2006 Thermodynamics and kinetics of cation ordering in natural and synthetic $Mg(Al, Fe^{3+})_2O_4$ spinels from *in situ* high-temperature x-ray diffraction *Am. Mineral.* **91** 306–12

Méducin F, Redfern S A T, Le Godec Y, Stone H J, Tucker M G, Dove M T and Marshall W G 2004 Study of cation order–disorder in $MgAl_2O_4$ spinel by *in situ* neutron diffraction up to 1600 K and 3.2 GPa *Am. Mineral.* **89** 981–6

Millard R L, Peterson R C and Hunter B K 1992 Temperature dependence of cation disorder in $MgAl_2O_4$ spinel using ^{27}Al and ^{17}O magic-angle spinning NMR *Am. Mineral.* **77** 44–52

Nakatsuka A, Ueno H, Nakayama N, Mizota T and Maekawa H 2004 Single-crystal x-ray diffraction study of cation distribution in $MgAl_2O_4$–$MgFe_2O_4$ spinel solid solution *Phys. Chem. Minerals* **31** 278–87

Nell J, Wood B J and Mason T O 1989 High-temperature cation distributions in Fe_3O_4–$MgAl_2O_4$–$MgFe_2O_4$–$FeAl_2O_4$ spinels from thermopower and conductivity measurements *Am. Mineral.* **74** 339–51

O'Neill H St C 1992 Temperature dependence of the cation distribution in zinc ferrite ($ZnFe_2O_4$) from powder XRD structural refinements *Eur. J. Mineral.* **4** 571–80

O'Neill H St C, Annersten H and Virgo D 1992 The temperature dependence of the cation distribution in magnesioferrite ($MgFe_2O_4$) from powder XRD structural refinements and Mössbauer spectroscopy *Am. Mineral.* **77** 725–40

O'Neill H St C and Dollase W A 1994 Crystal structure and cation distributions in simple spinels from powder XRD structural refinements: $MgCr_2O_4$, $ZnFe_2O_4$, Fe_3O_4 and the temperature dependence of the cation distribution in $ZnAl_2O_4$ *Phys. Chem. Minerals* **20** 541–55

O'Neill H St C and Navrotsky A 1983 Simple spinels: crystallographic parameters, cation radii, lattice energies, and cation distribution *Am. Mineral.* **68** 181–94

O'Reilly W 1994 Magnetic recording in nature: the medium, the mechanism and the message *J. Magn. Magn. Mater.* **137** 167–85

Pattrick R A D, van der Laan G, Henderson C M B, Kuiper P, Dudzik E and Vaughan D J 2002 Cation site occupancy in spinel ferrites studied by x-ray magnetic circular dichroism: developing a method for mineralogists *Eur. J. Minerals* **14** 1095–102

Pavese A, Artioli G, Russo U and Hose A 1999 Cation partitioning versus temperature in $(Mg_{0.70}Fe_{0.23})Al_{1.97}O_4$ synthetic spinel by in situ neutron powder diffraction *Phys. Chem. Minerals* **26** 242–50

Pearce C I, Henderson C M B, Pattrick R A D, van der Laan G and Vaughan D J 2006 Direct determination of cation site occupancies in natural ferrite spinels by $L_{2,3}$ x-ray absorption spectroscopy and x-ray magnetic circular dichroism *Am. Mineral.* **91** 880–93

Peterson R C, Lager G A and Hitterman R L 1991 Time-of-flight neutron powder diffraction study of $MgAl_2O_4$ at temperatures up to 1273 K *Am. Mineral.* **76** 1455–8

Princivalle F, Della Giusta A, De Min A and Piccirillo E M 1999 Crystal chemistry and significance of cation ordering in Mg–Al rich spinels from high-grade hornfels, Predazzo-Monzoni, NE Italy *Mineral. Mag.* **63** 257–62

Redfern S A T, Harrison R J, O'Neill H St C and Wood D R R 1999 Thermodynamics and kinetics of cation ordering in $MgAl_2O_4$ spinel up to 1600 °C from *in situ* neutron diffraction *Am. Mineral.* **84** 299–310

Reichmann H J and Jacobsen S D 2006 Sound velocities and elastic constants of $ZnAl_2O_4$ spinel and implications for spinel-elasticity systematics *Am. Mineral.* **91** 1049–54

Saito F, Toyoda T, Mori T, Tanaka M, Hirano K and Sasaki S 1999 Site- and valence-selective study on the origin of Fe peaks in magnetic circular dichroism of Ni ferrites, $Fe[Ni_xFe_{2-x}]O_4$ *Physica* B **270** 35–44

Schiessl W, Potzel W, Karzel H, Steiner M, Kalvius G M, Martin A, Krause M K, Halevy I, Gal J, Scafer W, Will G, Hillberg M and Wappling R 1996 Magnetic properties of the $ZnFe_2O_4$ spinel *Phys. Rev.* B **53** 9143–52

Šepelák V, Baabe D and Becker K D 2000 Mechanically induced cation redistribution and spin canting in nickel ferrite *J. Mater. Synth. Process.* **8** 333–7

Shannon R D 1976 Revized effective ionic radii and systematic studies of interatomic distances in halides and chalcogenides *Acta Crystallogr.* A **32** 751–67

Tanaka K, Makita M, Shimizugawa Y, Hirao K and Soga N 1998 Structure and high magnetization of rapidly quenched zinc ferrite *J. Phys. Chem. Solids* **59** 1611–8

Turkin A I and Drebushchak V A 2005 Cation distribution in $MgFe_2O_4$ versus pressure and temperature: experiments in a piston–cylinder apparatus *Am. Mineral.* **90** 764–7

Uchida H, Lavina B, Downs R T and Chesley J 2005 Single-crystal x-ray diffraction of spinels from the San Carlos Volcanic Field, Arizona: spinel as a geothermometer *Am. Mineral.* **90** 1900–8

Waychunas G A 1991 Crystal chemistry of oxides and oxyhydroxides *Rev. Mineral. (Min. Soc. Am.)* **25** 11–68

Waychunas G A, Apted M J and Brown G J Jr 1983 X-ray K-edge absorption spectra of Fe mineral and model compounds: near edge structure *Phys. Chem. Minerals* **10** 1–9

Wilke M, Farges F, Petit P-M, Brown G E Jr and Martin F 2001 Oxidation state and coordination of Fe in mineral: an Fe K-XANES spectroscopic study *Am. Mineral.* **86** 714–30

Winell S, Annersten H and Prakapenka V 2006 The high-pressure phase transformation and breakdown of $MgFe_2O_4$ *Am. Mineral.* **91** 560–7

Wood B J, Kirkpatrick R J and Montez B 1986 Order–disorder phenomena in $MgAl_2O_4$ spinel *Am. Mineral.* **71** 999–1006

Wright P A, Natarajan S, Thomas J M and Gai-Boyes P L 1992 Mixed-metal amorphous and spinel phase oxidation catalysts: characterization by x-ray diffraction, x-ray absorption, electron microscopy, and catalytic studies of systems containing copper, cobalt, and manganese *Am. Chem. Soc.* **4** 1053–65

Yang A, Harris V G, Calvin S, Zuo X and Vittoria C 2004 Extended x-ray absorption fine structure analysis of cation distribution in $MnFe_2O_4$ single crystal films and artificial ferrite structures *IEEE Trans. Magn.* **40** 2802–4

Yao T, Imafui O and Jinno H 1991 EXAFS study of cation distribution in nickel aluminate ferrites *J. Am. Ceram. Soc.* **74** 314–7